Development of Perovskite-type Oxide Cathode for Proton-conducting SOFC

Makiko ASAMOTO, Hiroyuki YAMAURA, and Hidenori YAHIRO

Abstract: The electrochemical performances of the perovskite-type oxide cathodes with uniform particles were investigated in H_2-O_2 SOFC system using proton conductor. Among the perovskite-type oxides used in the present study, $La_{0.7}Sr_{0.3}FeO_3$ (LSF) exhibited the lowest cathodic overpotential at the temperature as low as 773 K. The cathode performances of LSF depended on the heat-treatment temperature prior to electrochemical measurements. In addition, it was found that the overpotentials of LSF cathode and the activation energies of cathode reaction were influenced by the electrode morphologies such as particle size and uniformity. The structure and the electrical conductivity of the proton-conducting ceramic film fabricated on LSF electrode substrate are also presented.

Key words: Proton conductor, SOFC, perovskite-type oxide, cathode

1. Introduction

Several doped perovskite-type oxides such as Yb-doped $SrCeO_3$[1] and Nd- or Gd-doped $BaCeO_3$ [2, 3] belong to the group of solid state protonic conductors at high temperature and are of interest for their applications in hydrogen sensors [4], hydrogen pumps [5], membrane reactors [6], and fuel cells [7-10]. The use of proton-conducting electrolyte in solid oxide fuel cells (SOFCs) has some advantages compared with that of the oxide-ion conductor. For instance, the protonic ceramic fuel cells form water at the cathode compartment. It means that the fuel unreacted keeps pure at the anode compartment, requiring no recirculation. Iwahara and co-workers [7] reported the operation of a H_2-O_2 fuel cell using proton-conducting electrolyte, $SrCe_{0.95}Yb_{0.05}O_{3-\alpha}$ (SCY). Bonanos et al. [10] demonstrated that a H_2-O_2 fuel cell using $BaCe_{0.8}Gd_{0.2}O_3$ (BCG) electrolyte yielded a high current density. Recently, Coors [11] pointed out that the protonic ceramic fuel cell is ideal for use with hydrocarbon fuels such as natural gas.

The electrical conductivity of protonic ceramics was studied as a function of oxygen partial pressure [12]. In a hydrogen atmosphere corresponding to very reducing oxygen partial pressure, it is reported that the electrical properties of both SCY and BCG are dominated by the ionic conductivity at low temperature. The transition from ionic to electronic conductivity in a hydrogen atmosphere was observed at about 1023 K for SCY. This suggests

*Department of Materials Science and Biotechnology, Graduate School of Science and Engineering, Ehime University, Matsuyama, Japan.
E-mail: hyahiro@eng.ehime-u.ac.jp

原稿受理　平成 20 年 10 月 31 日

that SOFC using SCY electrolyte should be operated below 1023 K. However, the decrease in the operating temperature results in an increase of the overpotential, mainly at the cathode. Therefore, the development of a superior cathode becomes an important subject to realize an intermediate temperature-solid oxide fuel cell (IT-SOFC) using protonic-conducting electrolyte.

Mixed conducting ABO_3 perovskite-type oxides have received much attention as electrode materials in SOFC. $La_{1-x}Sr_xMnO_3$ has been considered to be one of the most promising cathode materials for oxide ion-SOFCs [13]. As alternative candidates, $La_{1-x}Sr_xCoO_3$ [14], $La_{1-x}Sr_xFeO_3$ [15], and $La_{1-x}Sr_xMn_{1-y}Co(Fe)_yO_3$ [16] have been reported. However, little is known about the perovskite-type oxide cathode in SOFC using proton conductor. This paper presents our recent results concerning the cathode performance of the perovskite-type oxide in H_2-O_2 fuel cell systems using SCY and $BaCe_{0.8}Y_{0.2}O_{3-\alpha}$(BCY) electrolytes exhibiting the proton conduction. In addition, the structure and the electrical conductivity measurements of BCY thin film fabricated on LSF electrode substrate are also presented.

2. Experimental

Polycrystalline SCY electrolyte used in the present study was prepared by conventional solid-state reactions [1]. The mixed powders were calcined at 1673 K for 10 h in air. The calcined oxides were ground and uniaxially pressed into pellets under a pressure of 2000 kg cm^{-2}. The obtained pellets were then sintered at 1773 K for 10 h in air. The diameter and the thickness of the sintered pellets were *ca.* 9 mm and *ca.* 2.3 mm, respectively. X-ray powder diffraction (XRD; RIGAKU RINT2000, CuK_α) patterns confirmed that the SCY sample exhibited a single phase with the perovskite structure.

Cathode materials, $La_{1-x}Sr_xMO_3$ (M = Mn, Fe, and Co), were prepared by the following solid-state reaction. La_2O_3 (Wako, 99.99%), $SrCO_3$ (Wako, 95%), $MnCO_3$ (Wako, 99%), Fe_2O_3 (Wako, 99.5%), and Co_3O_4 (Wako, >90%) were used as starting materials. These powders were mixed in appropriate ratios and ground in a ball mill with ethanol for 24 h. After drying, the mixed powders were calcined at 1673 K for 10 h in air. XRD measurements of $La_{0.7}Sr_{0.3}MO_3$ samples with various B-site cations yielded single phase XRD-patterns assigned to the perovskite-type structure; no diffraction peaks from a secondary phase or from the starting materials were observed. $La_{0.7}Sr_{0.3}MO_3$ oxide dispersed into turpentine oil (Wako, 90%) was painted on one face of electrolyte disk, dried at room temperature for several hours, and then heat-treated at 1173-1473 K for 3 h to obtain good adherence of the cathode to the electrolyte. The platinum was sputtered on the opposite side of the electrolyte as an anode.

The construction of a H_2-O_2 fuel cell was essentially the same as that reported elsewhere [17]. The electrolyte with electrodes was placed between silica tubes with glass gaskets to separate two compartments. A Pt wire was connected to a Pt-mesh current collector attached to each electrode. A Pt wire was wound around the side of the electrolyte disk as a reference electrode. Hydrogen gas saturated with water vapor at 298 K was supplied to the anode compartment at a flow rate of 50 $cm^3 \cdot min^{-1}$, while air as an oxidant gas was supplied to the cathode compartment at a flow rate of 50 $cm^3 \cdot min^{-1}$. A current interruption method using the reference electrode was employed to obtain overpotentials of the anode and the cathode under the operation of a H_2-O_2 fuel cell at 773-973 K. The transient behavior of the electrode potential was measured by an oscilloscope (IWATSU

SS-5510). In order to measure the overpotential at a wide range of the current density, a supplemental voltage (1.2-1.3 V) was added to the cell voltage by connecting a battery in series with the fuel cell.

3. Results and discussion

3.1 Cathode overpotentials of various perovskite-type oxides

The electrochemical performances were measured for the following fuel cell;

H_2, Pt | SCY | $La_{0.7}Sr_{0.3}MO_3$ (M = Mn, Fe, and Co; LSM, LSF, and LSC), O_2.

The I-V and I-P results are shown in figure 1. The thickness of the perovskite-type oxide electrode, which was confirmed by scanning electron microscopy (SEM), was around 0.2 mm because it was reported that the overpotentials are influenced by the thickness of electrode [18]. The best electrochemical performance was obtained when LSF was used as a cathode. The order of cathode overpotentials was LSF < LSM < LSC.

Yamamoto et al. [18] reported that the lowest cathode overpotential was achieved for the LSC electrode among the perovskite-type oxides, $La_{1-x}Sr_xMO_3$, for oxide ion-conducting SOFC. The most suitable cathode material for a proton conducting-SOFC may be different from that for an oxide ion conducting SOFC although all the perovskite-type oxides used in the present study were not optimized with regard to their microstructure and compatibility with the electrode.

The cathode overpotential of LSF was lower than that of the sputtered Pt. The cathode overpotential of the sputtered Pt is *ca.* 2 times larger than the anodic overpotential of the sputtered Pt at a current density of 7.5 $mA \cdot cm^{-2}$, while the cathode overpotential of LSF is comparable to that of the anodic overpotential of sputtered Pt. This is contrast to the usual an oxide ion conducting SOFC of which the cathode overpotential is much higher than anodic one.

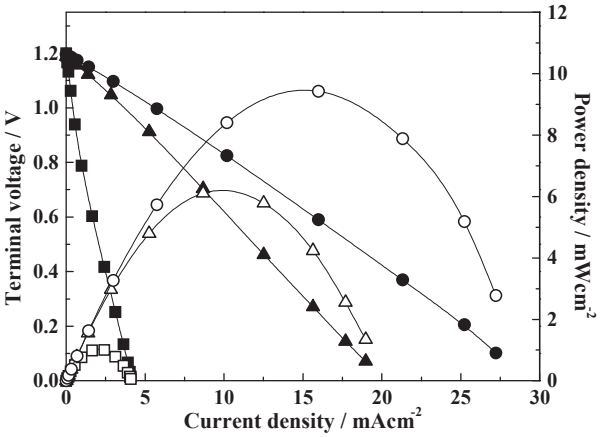

Figure 1. I-P (Δ, ○, □) and I-V (▲, ●, ■) carves for cells with LSM(Δ,▲), LSF (○, ●), and LSC(□, ■) cathodes.

3.2 Effect of Sr content and heat-treated temperature on the overpotential of LSF cathode

Since LSF showed the lowest overpotential among the various perovskite-type oxides, the cathode performance of LSF was investigated in more detail. The cathode overpotentials were dependent on Sr content, x, in $La_{1-x}Sr_xFeO_3$. The lowest overpotential was achieved at x = 0.3.

In order to obtain the good contact between electrode and electrolyte, the heat treatment is needed prior to the electrochemical measurement. It is well-known that the treatment at high temperature results in the strong adhesion between electrode and electrolyte, but simultaneously leads to the degradation of the electrochemical performance of electrode by the aggregation of electrode particles. Table 1 shows the influence of treatment temperature on cathode overpotential for the LSF electrode. It was demonstrated that the cathode overpotential increased with the increase in the treatment temperature from 1173 to 1473 K. From the SEM photographs, LSF particles heated at 1273 K are fine and the particle size increased gradually upon heating at higher temperature. This result suggests that the number (three-phase boundary length) of electrochemically active sites at the electrode/electrolyte interface becomes smaller with increasing treatment temperature.

Diffusion of metal ions leading to the chemical reaction at the electrode and electrolyte interface also causes degradation of the electrical properties. LSC and LSM were reported to react with YSZ to yield the poorly conducting La- and Sr-zirconate at the interface [19, 20], whereas LSF is thermally stable in contact with YSZ at 1673 K [21]. We examined the thermal reactivity of SCY and LSF by XRD diffraction analysis. Before heating, two sets of XRD peaks assigned to SCY and LSF were observed. After heating at 1173 K for 3 h in air, no significant change in both the peak intensity and the peak position occurred. However, upon heating at 1273 K, new peaks attributable to $SrLaFeO_4$ were observed and grew up at increasing temperature. Such a formation of a second phase may also be related with an increase in the overpotential of LSF. It is clear that the lower heating temperature is favorable in order to suppress the sintering of LSF cathode and preventing the formation of $SrLaFeO_4$. However, poor adherence of LSF cathode to the SCY electrolyte could be obtained below 1173 K. As a result, it was concluded that the optimum treatment temperature is 1173-1273 K.

Table 1 Cathodic overpotentials of LSF heat-treated at different temperature

Heat-treatment temperature / K	Cathodic overpotential / V
1173	0.052
1273	0.132
1373	0.232
1473	0.336

3.3 Influence of Particle Size of LSF Powder

The particle size distributions of $La_{0.7}Sr_{0.3}FeO_3$ (LSF) powders ground by ball-milling for 10 and 30 h are given in Fig. 2, together with that of as-calcined LSF powder. It is obvious that the LSF powders ground by ball-milling are more uniform and finer than as-calcined LSF powder. The mean diameters of LSF powders ground by ball-milling for 10 and 30 h were estimated to be 1.8 and 0.8 μm, respectively. The resulting LSF

powders were used to evaluate the cathodic performances in H_2-O_2 SOFC. Hereafter, the cathodes made from the LSF powders with the different distributions (A)-(C), as shown in Fig. 2, are represented by LSF (A)-(C), respectively.

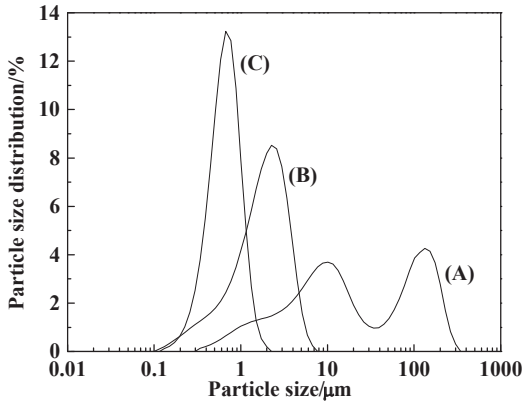

Figure 2. Particle size distribution of LSF powders (A) as-calcined at 1673 K and ground by ball-milling for (B) 10 and (C) 30 h.

Figure 3 represents the SEM photographs of interfaces between LSF cathode and SCY electrolyte. The morphologies of LSF (A)-(C) significantly differed from each other. We can see that the LSF (B) and (C) were less porous than LSF (A). This may be due to fine particles and good uniformity in particle size of LSF powder. In addition, it seems that LSF (B) and (C) tightly adhered to SCY electrolyte. This implies that there is a fair number of the three phase boundary in LSF (B) and (C).

The cathodic overpotentials of LSF (A)-(C) are depicted in Fig. 4. The overpotential of LSF cathode decreased in the following order: LSF (A) > (B) > (C). Thus, it was found that the cathodic overpotential in H_2-O_2 SOFC using proton conductor is strongly affected by the particle size and distribution of souse powder of cathode material.

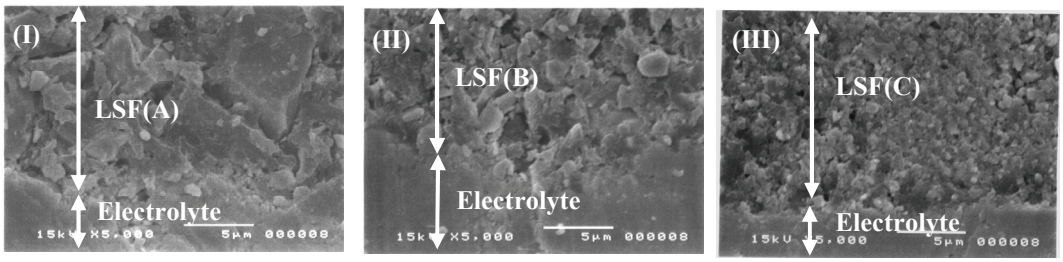

Figure 3. SEM photographs of interface between LSF cathode and SCY electrolyte. (I) LSF (A), (II) LSF (B), and (III) LSF (C).

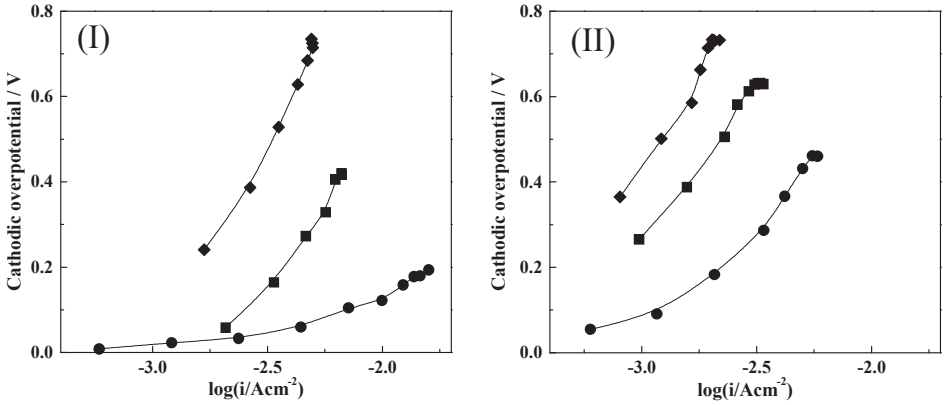

Figure 4. Cathodic overpotentials of (♦) LSF(A), (■) LSF(B), and (●) LSF(C) at (I) 773 K and (II)973 K.

The activation energy of electrode reaction can be calculated from the Arrhenius plot of the inverse of the electrode resistance corresponding to the slope of the overpotential against the current density [22]. The activation energies of LSF (A)-(C) are summarized in Table 2. The activation energy of Pt cathode was estimated to be 0.90 eV in the temperature range of 773-973 K, being close to the value (0.99 eV) reported by Uchida et al. [22]. As can be seen in Table 2, the activation energy of LSF cathode was clearly lower than that of Pt cathode. This result suggests that the rate-determining step of the electrode reaction for LSF cathode is different from that for Pt cathode.

Uchida et al. [22] suggested that the cathode reaction consists of the following five elementary steps and the surface diffusion of adsorbed oxygen atoms toward the electrochemically active sites on Pt (eq. (3)) is the rate-determining step.

$O_2(g) \rightarrow O_2(ad)$ (1)

$O_2(ad) \rightarrow 2O(ad)$ (2)

surface diffusion of O(ad) (3)

$O(ad) + 2H^+ + 2e \rightarrow H_2O(ad)$ (4)

$H_2O(ad) \rightarrow H_2O(g)$ (5)

On the other hand, we reported that the either eq. (4) or (5) in above elementary steps is the rate-determining step for LSF cathode [17].

As can be seen in table 2, the activation energies of LSF increased in the following order: LSF (A) < (B) < (C). This result suggests that the rate-determining step is changed by the electrode morphology. As can be expected from the SEM photographs in Fig. 3, the porosity of LSF cathode decreased in the following order: LSF (A) > (B) > (C), suggesting that the diffusion of water formed was limited in the same order. Therefore, for LSF (C), the desorption/diffusion of water (eq. (5)) is consider to be the rate-determining step. In the case of LSF (A), as the strict limitation of gas diffusion is moderated due to the presence of large-sized pore in electrode, the other

elementary step would become the rate-determining step.

Table 2 Activation energies of LSF (A), (B) and (C) cathodes

Cathode	Activation energy / eV
LSF (A)	0.36
LSF (B)	0.51
LSF (C)	0.71

3.4 Fabrication of BCY film on LSF substrate

The use of thin films rather than bulk materials is advantageous for reducing devise resistance and operating temperature. Several techniques such as MOCVD [23], a polymeric precursor spin coating [24], and a colloidal suspension spin coating [25], have been reported for preparing thin film of proton conductors. We attempted to fabricate a dense thin film by spin-techniques.

Polycrystalline BCY precursor powders for spin coating were prepared by the following evaporation-to-dryness method. The BCY powder was ultrasonically mixed with isopropanol for 60 min to form a homogeneous dispersion. The BCY powder-suspended solution was added dropwise onto a LSF substrate rotated at 7200 rpm. The sample was dried at room temperature and annealed at 1473-1573 K for 12 h. The coating-drying-annealing cycles were repeated several times. Here-in-after, the samples were abbreviated as BCY/LSF (1573, 3), where the numerical values in the parenthesis indicate the annealing temperature and the number of cycles.

Figure 5 shows SEM micrograph of cross-section of BCY/LSF (1573, 3) device. BCY thin film was dense and the thicknesse was about 1.7 μm. The thickness of BCY thin film was proportional to the number of the spin coating cycles: 0.5 and 1.7 μm for BCY/LSF (1573, 1) and BCY/LSF (1573, 3) devices, respectively. XRD pattern obtained for BCY/LSF (1573, 3) showed a weak peak assigned to the BCY at 2θ=28.7 degree. These results demonstrated the successful preparation of BCY thin film on LSF substrate.

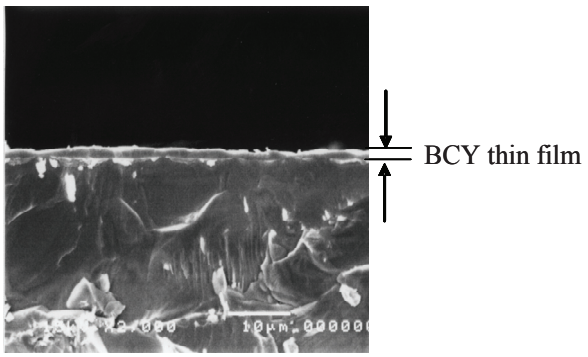

Figure 5. SEM image of cross-section of BCY/LSF(1573, 3).

The electrical conductivities of BCY/LSF (1573, 3) and BCY/LSF (1573, 7) devices are shown in figure 6 as a function of reciprocal temperature. The electrical conductivity for the bulk polycrystalline BCY specimen is also shown in this figure. The electrical conductivity of bulk BCY is about 1 and 2 orders of magnitude larger than those of BCY/LSF (1573, 3) and BCY/LSF (1573, 7), respectively. The large interfacial resistance between BCY thin film and LSF substrate may be due to the formation of the second phase with low electrical conductivity. The linear relationship between log electrical conductivity and reciprocal temperature was obtained for all samples, suggesting that the activation energy of electrical conduction remains unchanged in the temperature range of 873-1073 K. The activation energies were determined from the slop of each line to be 26.6, 45.3, and 57.3 $kJmol^{-1}$ for bulk BCY, BCY/LSF (1573, 3), and BCY/LSF (1573, 7), respectively, also suggesting the presence of the interfacial effect. Further studies to inhibit the chemical reaction between the dense thin film and the oxide substrate are in progress.

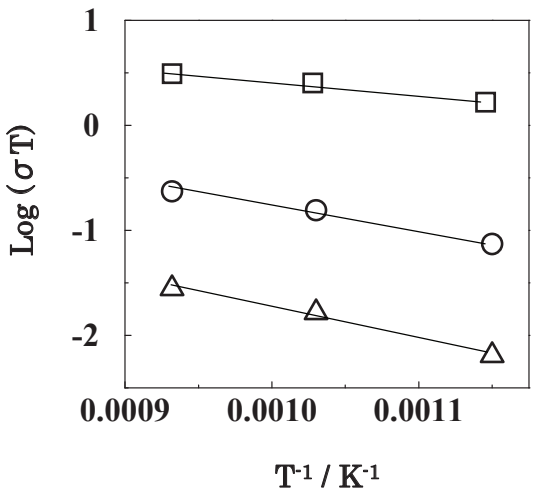

Figure 6. Electrical conductivities of (○)BCY/LSF(1575, 3), (Δ)BCY/LSF(1573, 7), and (□)bulk BCY as a function of reciprocal temperature.

4. Conclusions

The cathode polarization of perovskite-type oxide was investigated in the H_2-O_2 fuel cell using proton-conducting SOFC. The overpotential of LSF cathode was smaller than those of LSM and LSC. The best performance was achieved for LSF ($La_{0.7}Sr_{0.3}FeO_3$) treated at 1173-1273 K. The overpotentials of LSF cathode were influenced by the electrode morphologies such as particle size and uniformity; the decrease in the particle size resulted in the decrease in the overpotential. Dense BCY film could be fabricated by the spin coating on LSF electrode substrate. However, the problem still remains; the electrical conductivity of BCY film fabricated on LSF oxide substrate was lower than that of the bulk BCY due to the formation of a second phase with low conductivity at the electrolyte/electrode substrate interface.

References

[1] H. Iwahara, T. Esaka, H. Uchida, and N. Maeda: Proton conduction in sintered oxide and its application to steam electrolysis for hydrogen production, *Solid State Ionics* **3/4**, 359 (1981).

[2] J. F. Liu and A. S. Bowick: The incorporation and migration of protons in Nd-doped $BaCeO_3$, *Solid State Ionics* **50**, 131 (1992).

[3] H. Iwahara, H. Uchida, K. Ono, and K. Ogaki: Proton conduction in sintered oxides based on $BaCeO_3$, *J Electrochem. Soc.* **135**, 529 (1988).

[4] N. Kurita, K. Otsuka, N. Fukatsu, and T. Ohnishi: Measuring apparatus for hydrogen permeation using oxide proton conductor, S*olid State Ionics* **79**, 358 (1995).

[5] H. Iwahara: Technological challenges in the application of proton conducting ceramics, *Solid State Ionics* **77**, 289 (1995).

[6] S. Hamakawa, T. Hibino, and H. Iwahara: Electrochemical hydrogen permeation in a proton-hole mixed conductor and its application to a membrane reactor, *J. Electrochem. Soc.* **141**, 1720 (1994).

[7] H. Iwahara, H. Uchida, and M. Maeda: High temperature fuel and steam electrolysis cells using proron conductive solid electrolytes, *J. Power Sources* **7**, 283 (1982).

[8] H. Iwahara, H. Uchida, and S. Tanaka: High temperature type proton conductor based on $SrCeO_3$ and its application to solid electrolyte fuel cells, *Solid State Ionics* **9/10**, 1021 (1983).

[9] H. Iwahara, T. Yajima, T. Hibino, and H. Ushida: Performance of solid oxide fuel cell using proton and oxide ion mixed conductors based on $BaCe_{1-x}Sm_xO_{3-\alpha}$, *J. Electrochem. Soc.* **140**, 1687 (1993).

[10] N. Bonanos, B. Ellis and M. N. Mahmood: Construction and operation of fuel cells based on the solid electrolyte $BaCeO_3$:Gd, *Solid State Ionics* **44**, 305 (1991).

[11] W. G. Coors: Protonic ceramic fuel cells for high-efficiency operation with methane, *J. Power Sources* **118**, 150 (2003).

[12] N. Bonanos: Transport properties and conduction mechanism in high-temperature protonic conductors, *Solid State Ionics* **53-56**, 967 (1992).

[13] N. Q. Minh: Ceramic fuel cells, *J. Am. Ceram. Soc.* **76**, 563 (1993).

[14] H. Uchida, S. Arisaka, and M. Watanabe: High performance electrodes for medium temperature solid oxide fuel cells: Activation of $La(Sr)CoO_3$ cathode with high dispersed Pt metal electrocatalysts, *Solid State Ionics* **135**, 347 (2000).

[15] M. D. Anderson, J. W. Stevenson, and S. P. Simner: Reactivity of lanthanide ferrite SOFC cathodes with YSZ electrolyte, *J. Power Sources* **129**, 188 (2004).

[16] S. P. S. Badwal, S. P. Jiang, J. Love, J. Nowotny, M. Rekas, and E. R. Vance: Chemical diffusion in perovskite cathodes of solid oxide fuel cells: the Sr-doped $LaMn_{1-x}M_xO_3$ (M=Co. Fe) systems, *Ceram. International* **27**, 419 (2001).

[17] H. Yamaura, T. Ikuta, H. Yahiro, G. Okada: Cathodic polarization of strontium-doped lanthanum ferrite in proton-conducting fuel cell, *Solid State Ionics* 176, 269 (2005).

[18] O. Yamamoto, Y. Takeda, R. Kanno, M. Noda: Perovskite-oxides as oxygen electrodes for high temperature oxide fuel cell, *Solid State Ionics* **22**, 241 (1987).

[19] Y. Takeda, R. Kanno, M. Noda, Y. Tomida, and O. Yamamoto: Cathodic polarization phenomena of perovskite oxide electrodes with stabilized zirconia, *J. Electrochem. Soc.* **134**, 2657 (1987).

[20] F. M. Fiqueiredo, J. A. Labrincha, J. R. Frade, and F. M. B. Marques: Reaction between a zirconia-based electrolyte and $LaCoO_3$-based electrode materials, *Solid State Ionics* **101-103**, 343 (1997).

[21] S. P. Simner, J. P. Shelton, M. D. Anderson, J. W. Stevenson: Interaction between $La(Sr)FeO_3$ SOFC cathode and YSZ electrolyte, *Solid State Ionics* **161**, 11 (2003).

[22] H. Uchida, S. Tanaka, and H. Iwahara: Polarization at electrodes of a fuel cell with a high temperature-type proton conductive solid electrolyte, *J. Appl. Electrochem.* **15**, 93 (1985).

[23] M. Pan, G. Y. Meng, C. S. Chen, D. K. Peng, and Y. S. Lin: MOCVD synthesis of yttria doped perovskite type $SrCeO_3$ thin films, *Mater. Lett.* **36**, 44 (1998).

[24] I. Kosacki and H. U. Anderson: The structure and electrical properties of $SrCe_{0.95}Yb_{0.05}O_3$ thin film protonic conductors, *Solid State Ionics*, **97**, 429 (1997).

[25] S. Hamakawa, L. Li, A. Li, and E. Iglesia: Synthesis and hydrogen permeation properties of membranes based on dense $SrCe_{0.95}Yb_{0.05}O_{3-\alpha}$ thin films, *Solid State Ionics* **48**, 71 (2002).